Arctic Sea Ice Microstructure Observations Relevant to Microwave Scattering

MOHAMMED E. SHOKR[1] and NIRMAL K. SINHA[2]

ABSTRACT. Sea ice microstructure characteristics relevant to ice microwave scattering were studied during SIMMS'91 field experiment in Resolute Bay in May/June 1991. Thin sections of the top 300 mm layer of first-year and multi-year ice (from hummocks and melt ponds) were prepared and examined. Analysis is based mostly on qualitative observations, although statistics on bubble dimensions and geometry were obtained from digital analysis of thin section photographs. First-year ice featured mostly an oriented columnar grain structure. Both spherical and needle-shaped brine pockets were observed. In multi-year ice, a variety of grain structures and inclusion patterns were observed from the same floe. Hummock and melt pond ice are different in terms of grain structure and air bubble contents. Air bubbles in hummock ice are highly random and interconnected, especially near the surface. At lower depths, they retain simpler shapes and become oriented parallel to the dominant grain growth direction. In melt pond ice, two types of air inclusions whose typical dimensions differ by an order of magnitude were observed. Significant spatial variability of multi-year ice microstructure within a single floe is demonstrated.

Key words: sea ice, ice microstructure, ice microwave scattering, SAR ice signatures, air bubbles in sea ice

RÉSUMÉ. Au cours de l'étude de terrain SIMMS'91 menée dans la baie Resolute en mai/juin 1991, on a étudié les caractéristiques de la microstructure de la glace de mer pertinentes à la diffusion d'hyperfréquences par la glace. On a préparé et examiné de fines coupes transversales prélevées dans les 300 mm supérieurs de la glace de l'année et de la glace pluri-annuelle (provenant de hummocks et de mares de fonte). L'analyse s'appuie principalement sur des observations qualitatives, bien que les statistiques sur les dimensions et la géométrie des bulles aient été obtenues à partir du traitement numérique de photographies représentant de fines coupes transversales. La glace de l'année affichait principalement une structure granulaire prismée. On a observé des poches de saumure sphériques ainsi qu'aciculaires. Dans la glace pluri-annuelle, on a observé dans le même floe une diversité de structures granulaires et de schémas d'inclusion. Les hummocks et la glace des mares de fonte diffèrent quant à leur structure granulaire et au contenu des bulles d'air. Dans la glace de hummock, les bulles d'air sont distribuées au hasard et reliées entre elles, surtout près de la surface. À de plus grandes profondeurs, elles conservent des formes plus simples et s'orientent parallèlement à la direction dominante de la croissance granulaire. Dans la glace des mares de fonte, on retrouve deux types d'inclusions d'air dont les dimensions typiques diffèrent d'un ordre de grandeur. On démontre qu'il existe une importante variabilité spatiale de la microstructure de la glace pluri-annuelle à l'intérieur d'un même floe.

Mots clés: glace de mer, microstructure de la glace, diffusion d'hyperfréquences par la glace, signatures de la glace obtenues avec le RALS, bulles d'air dans la glace de mer

Traduit pour la revue *Arctic* par Nésida Loyer.

INTRODUCTION

Sea ice is a heterogeneous mixture of pure ice crystals, gas (air) bubbles and brine pockets in either liquid or solid forms. Several studies on microstructure of laboratory-made saline ice have been conducted to understand its formation and growth processes (Weeks and Assur, 1963; Weeks and Lofgren, 1967; Cox and Weeks, 1975). Only a few studies, however, have been conducted to relate the microstructure of natural first-year ice to the growth rate and the meteorological and oceanographical conditions (Nakawo and Sinha, 1981, 1984). Most studies focus on the fabric of crystalline structure in relation to the ice age and the region of origin.

Peyton (1966) studied the structure of columnar ice 0.5 m or more beneath the surface of ice along the Alaskan coast and found that it was characterized by a strongly c-axis orientation in the horizontal plane. Strongly preferred c-axis orientation was also noticed by Sinha (1977) to occur within 20 mm below the surface in Strathcona Sound, Baffin Island, Canada. Photographs of highly oriented grains and intragranular salt inclusions are presented in the same reference. Weeks and Gow (1978) noted oriented columnar ice in the northern part of Alaska in land-fast ice and concluded that the alignment was related to the dominant orientation of water current under the ice cover. Sinha (1984) found the same structure in first-year and multi-year ice in Crozier Channel in the Beaufort Sea region. About 70% of the first-year ice adjacent to the east coast in Mould Bay (Canadian Western Arctic) was found to be vertically-oriented frazil ice with the c-axis of crystals randomly oriented in the horizontal plane (Sinha, 1986). This was attributed to the strong westerly wind during the formation of the ice cover. Tucker *et al.,* (1987) reported that about 75% of first-year ice in Fram Strait (between

[1] Atmospheric Environment Service, 4905 Dufferin Street, North York, Ontario M3H 5T4, Canada
[2] Institute for Engineering in the Canadian Environment, National Research Council of Canada, Ottawa, Ontario K1A 0R6, Canada

the East Greenland coast and Svalbard) consisted of columnar grains and the remaining 25% consisted of granular ice. Eicken and Lange (1989) studied three wind-controlled ice formation regimes in the Weddell Sea, where columnar ice predominated in undeformed ice (formed at low wind speeds), while granular ice predominated in heavily ridged and rafted ice (formed under high wind speeds). The lack of ice crystal orientation in the Sea of Bothnia as compared to ice in the Arctic Ocean was attributed by Weeks *et al.,* (1990) to the weaker or more variable sea current. Few studies have been carried out on characteristics of inclusions in ice (Poe *et al.,* 1974; Bjerkelund *et al.,* 1985)—a subject of direct relevance to ice microwave remote sensing.

Sea ice monitoring for operational and scientific applications has progressed through the use of advanced remote sensing tools, particularly in the microwave band. Both active and passive sensors have been used. The prime sensor within the category of active sensors is the Synthetic Aperture Radar (SAR) (Ulaby *et al.,* 1986). Interpretation of sea ice SAR images depends on understanding the radar backscattering mechanism. Extensive data on radar backscattering from ice at different frequencies are presented in the literature (e.g., Onstott, 1992). Backscattering is influenced by three factors: the ice surface roughness, the average dielectric constant of ice, and the microstructural properties of ice in terms of crystal structure and, more importantly, inclusions in ice. The third factor is the subject of this study.

Data on ice microstructural properties relevant to ice microwave remote sensing have become more available recently. Tucker *et al.,* (1991) presented results from surface-based active and passive microwave measurements, made in conjunction with physical and structural properties of ice. They showed that microwave signatures are affected by brine (liquid content) as well as gaseous void distribution. Eicken *et al.,* (1990) demonstrated the feasibility of quantitative texture analysis of ice microstructure images. Samples of different ice grain textures were distinguished based on the slope of the histogram of a texture parameter. Perovich and Gow (1991) calculated the correlation function between a template representing the typical appearance of brine pockets and the images of actual brine pockets in first-year ice. Statistics derived from the correlation function were ascribed to geometrical characteristics of brine pockets.

From the operational and scientific viewpoints, first-year and multi-year ice are among the most important ice types. For these types, the dominant inclusions are brine pockets and air bubbles respectively. Air bubbles exist at depths above the water level. The saline-free nature of the upper layer of multi-year ice allows more microwave energy to penetrate and interact with air bubbles. This interaction invokes volume scattering, which, together with surface scattering, forms the total backscatter received by a microwave remote sensor. Both experimental studies and microwave scattering model results (Gogineni *et al.,* 1990) show that volume scattering from first-year ice is not significant, particularly at small incidence angles of the incoming radiation. Modeling volume scattering in multi-year ice depends on information on bubble characteristics. At present, this information is scarce in the literature. Attempts to measure bubble dimensions are presented in Poe *et al.,* (1974) and

Bjerkelund *et al.,* (1985). The latter reference shows that 83% of the spherical bubbles in a horizontal section from completely desalinated second-year ice have a diameter less than 1 mm. More detailed study is required to explore the variability of bubble characteristics in relation to the topography of ice (i.e., hummock and melt pond), as well as the grain structures that commonly exist in each type. A requirement for *in situ* data to characterize inclusions that can be incorporated in microwave scattering models has been identified in the literature (e.g., Winebrenner *et al.,* 1989).

The present study was carried out to characterize air bubbles and brine pockets in relation to grain structures in natural sea ice in the Arctic. The study focused on differences between crystalline structure in hummocks and melt ponds. Results are based mostly on qualitative analysis, although limited quantitative information on air bubbles in multi-year ice is obtained from digital analysis of thin sections. The main objective of the study is to further define the parameters contributing to the microwave volume scattering. Hence, a better capability to interpret radar ice signatures observed in SAR images can be developed.

METHODS

The present study was the second in a series conducted under the Sea Ice Monitoring and Modeling Site (SIMMS) program. It was designed to collect baseline geophysical data from snow-covered sea ice and relate them to ice signatures from SAR (Barber, 1991).

The field study was conducted during 21 May to 4 June, 1991 in Resolute Passage off Barrow Strait, Northwest Territories, Canada (Fig. 1). This period signals the early melt season when the snow cover becomes wet but is not yet flooded (Livingstone *et al.,* 1987). In addition to ice microstructure data, *in situ* data such as thickness, surface roughness distribution, temperature and salinity profiles were collected on snow and ice. Some of these data are presented in other papers in this issue. Full documentation of the data are included in Reddan *et al.,* 1991.

The observation area consisted mainly of first-year sea ice with a number of relatively small (less than 2 km diameter) multi-year ice floes. The floes were located approximately 25 km west of Resolute Bay. An image of the observation area acquired by the STAR-2 SAR system (Nichols *et al.,* 1986) is shown in Fig. 2.

Core Sampling and Sectioning

Ice cores of 100 mm diameter were collected using an NRCC-made fibreglass core auger. Only the top 300 mm length of each core was examined. This is enough depth to include the penetration of the microwave C-band (estimated by Vant *et al.,* (1978) to be in the order of a few centimetres) and to accommodate the most effective part of penetration in multi-year ice (the penetration depth is reported by Fung and Eom (1982) to be around 1 m). Two cores were collected from each of the first-year ice (FYI) and PA1 (Passage) sites. Seven cores were collected from hummocks and five cores from melt ponds, all from the multi-year ice (MYI) site. Cores were transferred to a cold room at the
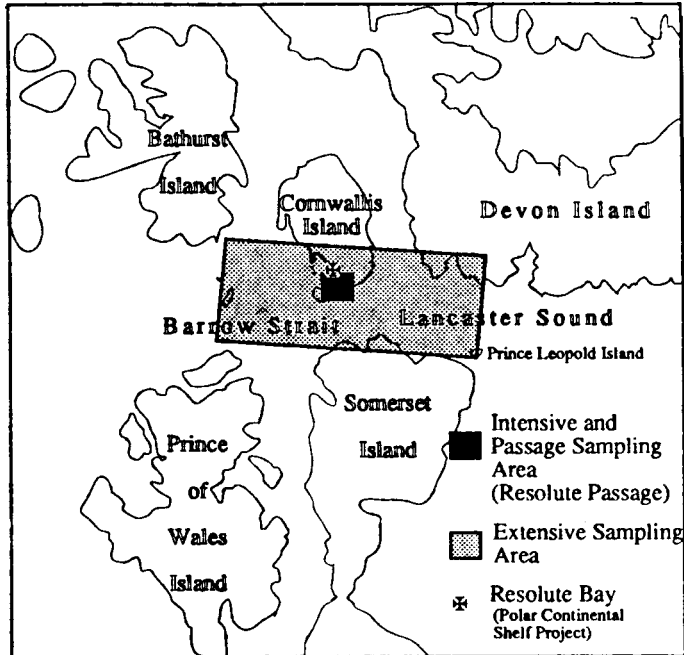
FIG. 1 Site of SIMMS'91 experiment.

FIG. 2. SAR image of the observation area, acquired 10 January 1991, showing sampling sites. MYI is a multi-year ice site; PA1, PA3, and HOME are first-year smooth ice sites; FYI, PA2 and RIDGE are first-year rough ice sites. The image coincides with the Intensive Sampling Area shown in Fig. 1. Scale: 1cm = 1.66 km.

base camp within two hours of sampling. They were stored at a temperature of -22°C. The cores were transferred as required (2 to 8 days later) to a cold laboratory adjacent to the cold room. Most thin sections were prepared at a temperature of -10°C. Lower temperatures, however, were required when thin sectioning the highly saline first-year ice cores.

Thin sections were prepared using the "Double Microtoming Technique" described in Sinha (1977). Two vertical sections were made from each core: one from the ice surface to about 140 mm depth, and the other from 150 to 290 mm depth. Five horizontal sections were made from each core at depths of 20 mm, 50 mm, 90 mm and 140 mm. Thin section preparation involved cutting a thick section (approximately 4 mm thick) on a band saw, and then thinning it to approximately 0.6 mm using a microtoming machine. Thinning was achieved by removing layers from one side only. When reaching the desired thickness, that side was then smooth and the thin section was flipped to remove layers from (i.e., to smooth) the other side. Thin sections were then photographed between parallel and crossed polarizers and in diffuse/scattered light using side illumination (Sinha, 1977). The parallel and crossed polarizers reveal crystal structure of ice, while diffuse light enhances the appearance of air and brine inclusions in the crystalline matrix.

Digital Analysis of Thin Section Photographs

Slides of vertical thin sections of the upper 140 mm depth of multi-year ice were digitized into an array of 1330×900 pixels. The slides were photographed under diffuse light so that the digital images contain bright objects (representing inclusions in the ice) within a dark background. A digital image analysis technique was developed to identify bubbles and to measure three geometrical parameters of each bubble. The parameters are:
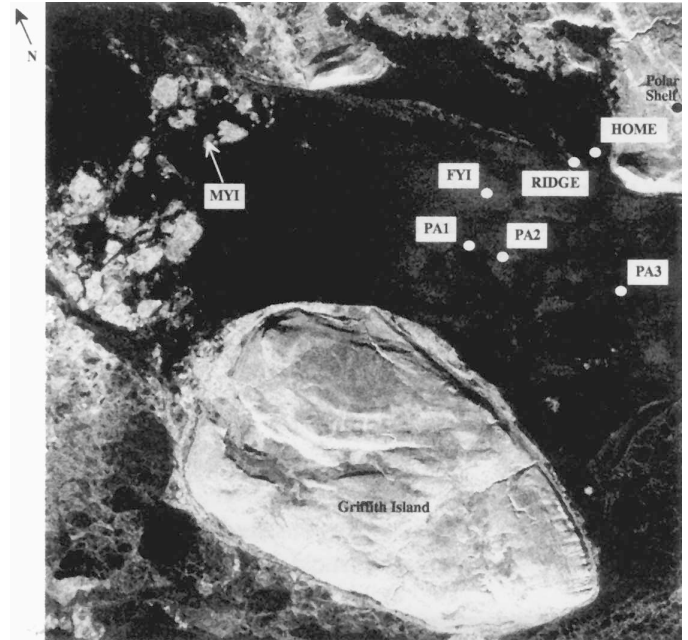
(1) The circle-equivalent diameter, a measurement of bubble size, defined as:

$$D = \sqrt{(4A/\pi)}$$

where A is the bubble area measured in pixels.

(2) The normalized compactness factor, a measurement of bubble shape, which is defined as:

$$C = A / (0.0795 \, P^2)$$

where P is the bubble perimeter. The ratio A/P^2 has its maximum value ($1/4\pi = 0.0795$) for a circle. Hence, C is a measure of the deviation of a bubble cross section shape from a perfect circle. As C approaches 1, bubbles become more circular, and as it approaches 0, bubbles become very narrow relative to their length.

(3) The distance "d", from a given bubble to the nearest bubble.

The technique was implemented on a Sun Workstation using EASI/PACE image analysis software. To simplify the analysis, we assumed that only air inclusions existed in multi-year ice. Brine pockets were considered to be negligibly small in number and size. Therefore, bright objects in the images were assumed to represent air bubbles. They were identified in the images using an appropriate threshold of grey tone. The threshold was selected such that the summation of bubble areas in a thin section image should be equal to the air volume fraction in the core segment

represented by that section. The technique identifies separated bubbles. Overlapping bubbles have to be separated manually, i.e., in an interactive mode. The smallest bubble that can be resolved in an image has a circle-equivalent diameter of 0.1 mm. This is an adequate resolution for the purpose of ice/microwave studies where the wavelength of the incident signal is typically a few centimetres. Details about the technique are presented in Shokr and Sinha (in press).

RESULTS AND DISCUSSION

First-year Ice Microstructure

The top surface layer (140 mm) of first-year ice in Resolute Passage during 1991 winter season consisted mainly of oriented columnar crystals. A typical vertical section of that layer is shown in two photographs, Figs. 3a and 3b, taken between cross polarizers and in diffuse light respectively. The section was prepared from a core collected from the FYI site, which had a relatively bright signature in the SAR image (Fig. 2) compared to signatures from other first-year ice sites. Brine inclusions can be seen in Fig. 3a located along grain and sub-grain boundaries.
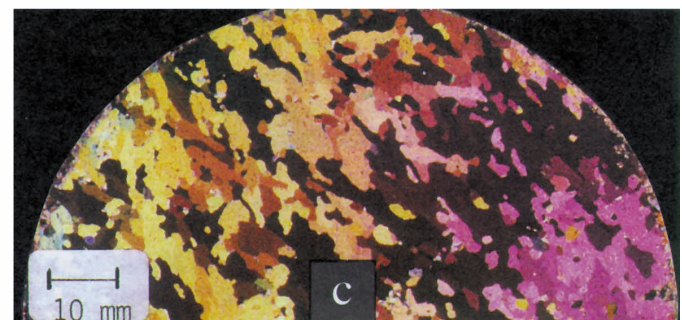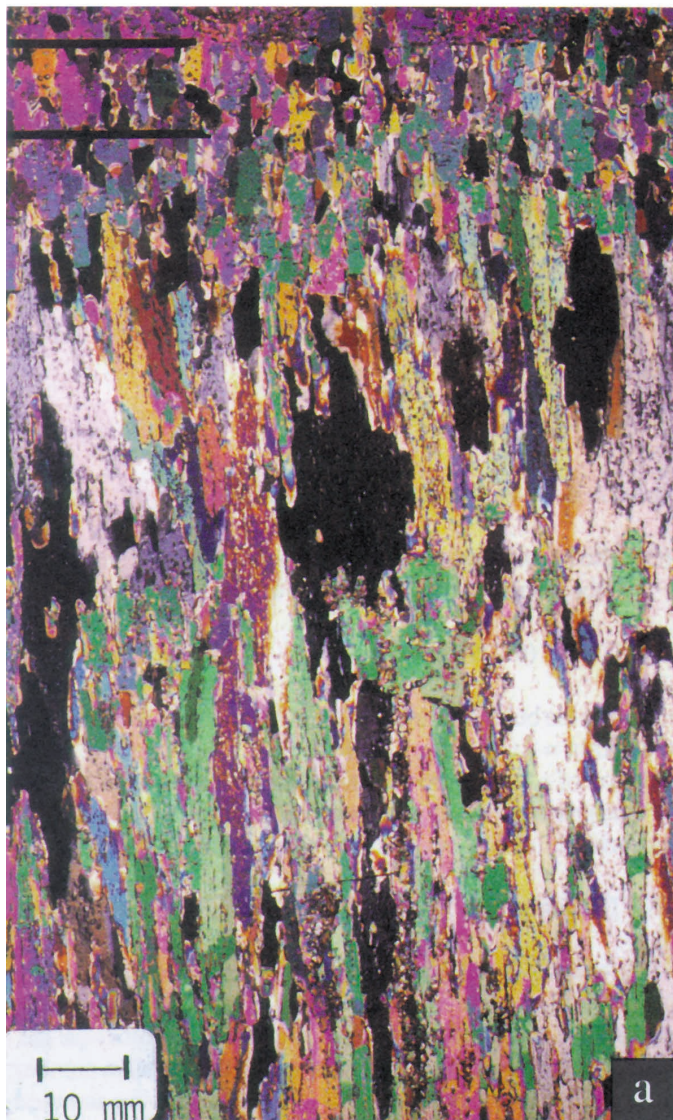

FIG. 3. First-year ice microstructure: (a), (b) vertical section of the upper 140 mm, photographed between crossed polarizers and in diffuse light respectively; (c) horizontal section at 140 mm depth photographed between crossed polarizers. Arrows at the top mark spots of high concentration of inclusions within the frazil ice matrix. The arrow at the bottom marks a vertical drainage channel. The horizontal dark lines in (a) divide layers of different microstructure characteristics.

Three sub-layers exhibiting different microstructural characteristics can be identified in the figure (their boundaries are marked with heavy dark lines). The first layer occupies the top 7 mm. It is characterized by randomly oriented fine grains typically a few millimetres in size. This layer constitutes slush ice formed, perhaps, during a snowfall. A high concentration of inclusions can be seen in two bright spots (marked with arrows in Fig. 3b). The second layer extends from 7 mm to 25 mm depth. It contains vertically-oriented frazil grains, slightly larger than those in the first layer. This is confirmed from the horizontal section at 20 mm (not shown). The grain size is typically 4 mm to 10 mm. Inclusions of different shapes can be seen. For frazil ice, the assumption of spherical inclusions proved to be appropriate for modeling the dielectric constant (Shokr and Sinha, in press). The inclusion dimensions range between a fraction of a millimetre to a maximum of 2 millimetres. These inclusions are a mix of gas and brine pockets. The size of the inclusions (gas and brine) decreases with the decrease in temperature. The volumetric change in the gaseous inclusions is primarily controlled by the thermal contraction of the ice volume. The decrease in the brine volume with temperature, on the other hand, is mainly controlled by the changes in the equilibrium conditions, which cause more solid salts to precipitate (Weeks and Akley, 1982). This elicits a decrease in the ice dielectric constant and an increase in microwave penetration depth, based on calculations reported by Shokr and Sinha (in press) from using the dielectric mixing model developed by de Loor (1968). Qualitatively speaking, more volume scattering is expected from first-year ice as ice temperature decreases.

The third layer features columnar-grained ice. Columns grow in the direction of maximum heat flux, which is usually vertical as shown in Fig. 3a. Brine pockets are arranged in a significant number of thin vertical lines. A brine drainage channel of approximately 4 mm width can be seen in the middle part of Fig. 3b. The grains are also oriented in the horizontal plane as shown in Fig. 3c, which represents a horizontal section of half core at 140 mm. The c-axis of the grains tends to be parallel to the dominant ocean current at the time of ice formation (Weeks and Gow, 1978; Nakawo and Sinha, 1984). Perhaps more relevant to microwave scattering, grain orientation also defines the direction along which brine pockets are stretched. Information on this direction, with respect to the applied electric field, is important to determine both dielectric constant and microwave scattering. This is especially true when brine pockets have an asymmetric cross section in the horizontal plane (as usually observed at depths below approximately 50 mm).

Multi-year Ice Microstructure

The surface of a multi-year ice floe is characterized by hummocks, melt ponds and ridges. In hummock ice, the only inclusion type is air bubbles. In melt pond ice and in the bulk of the ice, air bubbles and brine pockets coexist depending upon the salinity of the ice. Microwave volume scattering is more significant in hummocks because of their desalinated nature, which allows more energy penetration. Air bubbles are the main scatterer in both ice types. However, bubble formation mechanisms and geometrical characteristics are different between the two types.

Hummock Ice

Four cores from the same multi-year floe (MYI in Fig. 2) demonstrated a variety of grain structure. The shape and size of the grains indicate the conditions under which the ice was formed. The formation histories affect bubble shapes and orientations.

Figs. 4a and 4b depict a vertical section of the top 140 mm of core #1 from a hummock. The top part of the original core was white in colour and could have been mistaken as compacted snow or highly porous recrystallized ice. Because of earlier experience (Sinha, 1984), the top section was thin-sectioned with great care. The section shows large, vertically-oriented columnar grains starting immediately from the surface. This was the bulk ice that had existed below the surface layer in the original first-year ice prior to surface melt. No additional (i.e., newer) ice was formed on the hummock surface in subsequent seasons. Note the large number of air bubbles in Fig. 4b (the horizontal line shows a crack formed during the microtoming process). The measured density from this core, averaged over the 140 mm depth, was 0.620 kg·mm^{-3}.

Bubbles are highly interconnected near the surface. They lose their individual identity and form a complicated network. Photomicrography of air bubbles confirmed this observation. Therefore, the commonly-used assumption of elliptical bubble shape (used in microwave scattering models) may not be valid for the surface layer of multi-year ice. Dark areas appearing at corresponding locations in Figs. 4a and 4b represent large voids of a few millimetres in diameter. These voids have been observed occasionally. Statistics on their geometrical properties, though important for microwave scattering models, cannot be obtained from the present data because of the limited number of core samples. Since the average density was 0.620 kg·mm^{-3}, the corresponding air volume fraction was 38% (Shokr and Sinha, in press). This value is too high for air to be considered as an inclusion in a host (pure ice) material. This limits the application of dielectric and microwave scattering models based on the concept of inclusions contained in a host material of dominant volume fraction.

The second core was characterized by inclined columnar-grained ice. Figs. 5a and 5b show a vertical section from 140 to 280 mm depth. Large grains are readily visible. Their major axis varies from 50 to 80 mm, although smaller dimensions, around 10 mm, are observed near the top. Grains have irregular boundaries, which means that the original ice was highly saline. The large deviation of grain orientation from the vertical direction indicates that the hummock was part of an old rubble field. The boundary between bubble-rich/bubble-free regions is well identified at about 220 mm below the surface (it separates the bright objects and the dark background in Fig. 5b). This abrupt termination of air bubbles is observed in all hummock cores at depths between 50 and 350 mm.

The horizontal section at a 90 mm depth shows definite grain orientation as can be seen in Figs. 5c and 5d. Air bubbles are stretched and spatially arranged parallel to the dominant grain orientation. This implies that when surface melt infiltrates ice (in summer), the melt water follows paths connecting brine pockets
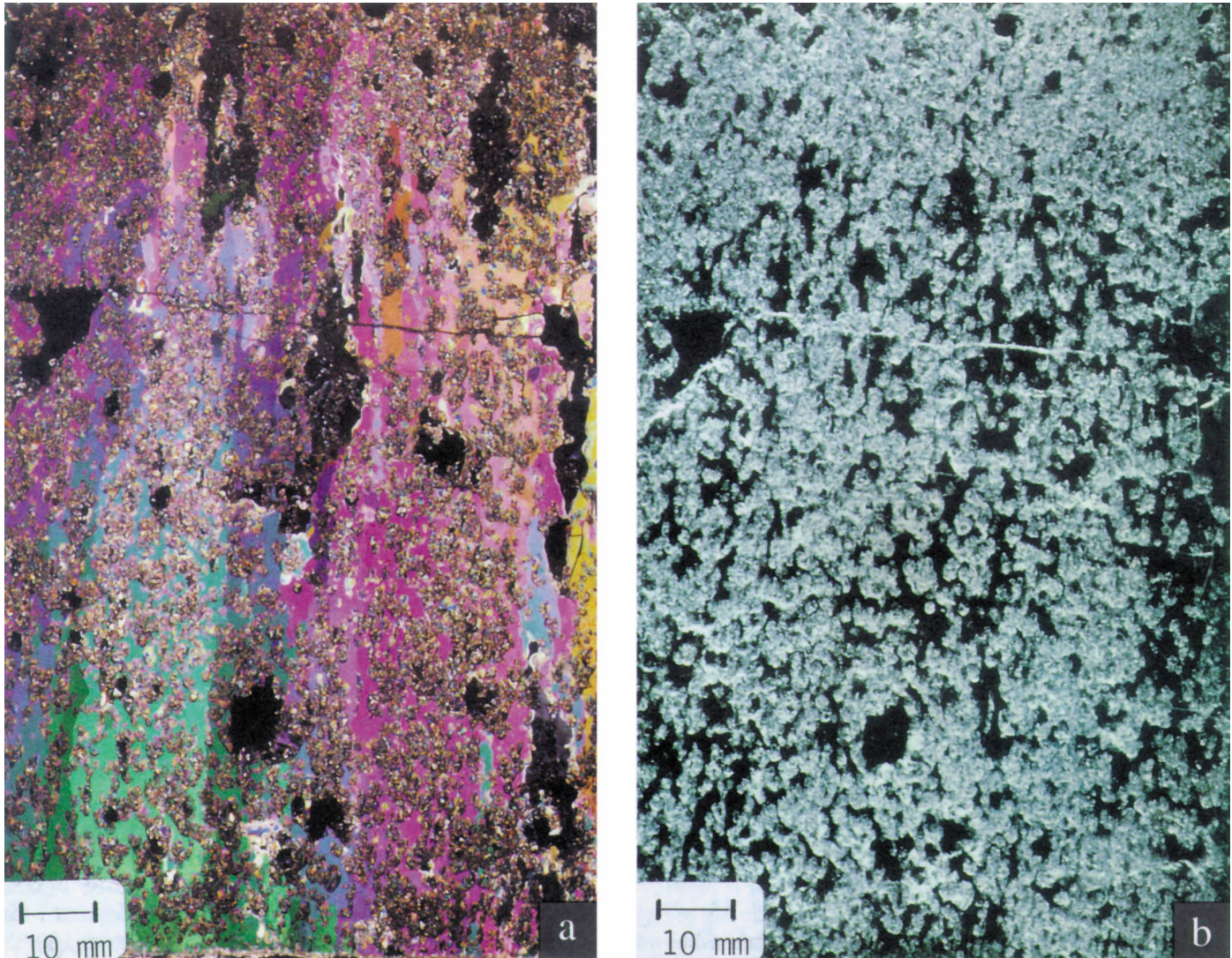
FIG. 4. Hummock core #1. Vertical section of the upper 140 mm depth, photographed (a) between crossed polarizers, (b) in diffuse light.

(which exist in the original saline first-year ice). The major axis of bubbles observed in this section varies from 1 to 6 mm long.

Fig. 6 shows the top 140 mm of core #3, featuring large oriented grains with straight boundaries. The planer boundaries, with no sub-grain boundaries, indicate that the ice grew from freshwater. Note that the long axis of the grains is inclined at approximately 45°. Since the long axis of the grains marks the growth direction or the direction of maximum heat flow, this ice must have grown at the edge of a melt pond and, thereby, on a side of a hummock. Note, however, that the ice contains vertically-oriented bubbles; i.e., not parallel to the dominant grain orientation. These bubbles were not, therefore, formed during the growth season. The bubbles trapped during growth are usually elongated with their long axis parallel to the grain growth direction. The ice under examination must have gone through another melt season after formation. Vertically-oriented air bubbles are indicators of the flow of melt water following the gravity (vertical) direction. This is the natural path of surface melt water to percolate through ice. Irregular and interconnected bubbles, with typical dimensions between 1 to 4 mm, are observed in the surface layer (top part of Fig. 6). At greater depths (bottom part of the figure), the common bubble shape is elliptical with typical dimensions of the major and minor axes being about 6 mm and 3 mm respectively. Bubbles are randomly spaced in both vertical and horizontal sections but they tend to cluster as shown in the figure. This aspect is not limited to this core and is being further examined.

The fourth core is characterized by small non-oriented grains a few millimetres in diameter throughout its entire length (280 mm). Fig. 7 is a vertical section between 150 and 280 mm depth. Based on its textural appearance, the top of the core is believed to comprise snow ice. The shape and distribution of air bubbles (dimensions between 2–5 mm) are similar to those observed in previous cores (Figs. 5, 6). Diffused-light photographs show that air bubbles terminate at about 130 mm depth (above the top edge of the shown section). The most important feature in this core is the large void, the black object with an approximate diameter of 62 mm, that can be seen in the top half of the photograph.
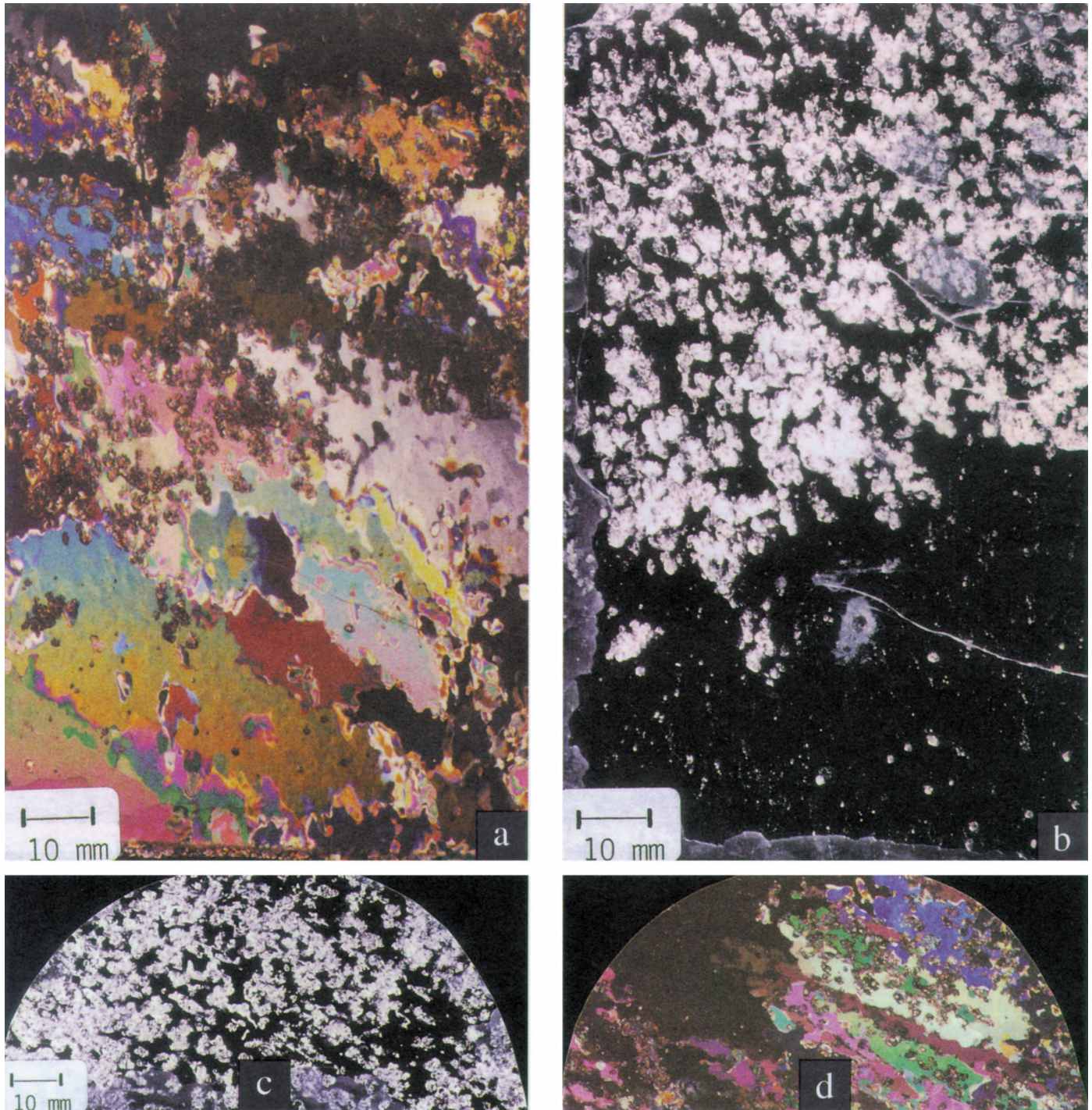
FIG. 5. Hummock core #2. (a), (b) vertical section of a depth range 140 mm to 290 mm, photographed between crossed polarizers and in diffuse light respectively. (c), (d) horizontal section at 90 mm depth photographed in diffuse light and between crossed polarizers respectively.

Melt Pond Ice

As with hummock ice, melt pond ice exhibits a variety of microstructure patterns. Unlike hummock ice, however, two distinct types of air inclusions exist in melt pond ice. The first, in the form of clusters of bubbles, is believed to originate from air entrapped between snow grains. These large clusters were consistently found in snow-ice layers forming the top layer of an ice cover. This layer is formed during freezing of snow slush or of waterlogged snow deposited on a pond. The second is small air bubbles trapped in the water or rejected during formation of ice in the pond. Both types differ from air bubbles in hummock ice in terms of formation mechanism and geometrical characteristics. Observations from three melt pond cores are presented in the following.

The typical structure of melt pond ice is shown in Fig. 8 (core #1), where a vertical section of the upper 140 mm depth is shown in Figs. 8a and 8b and a horizontal section at 90 mm depth is
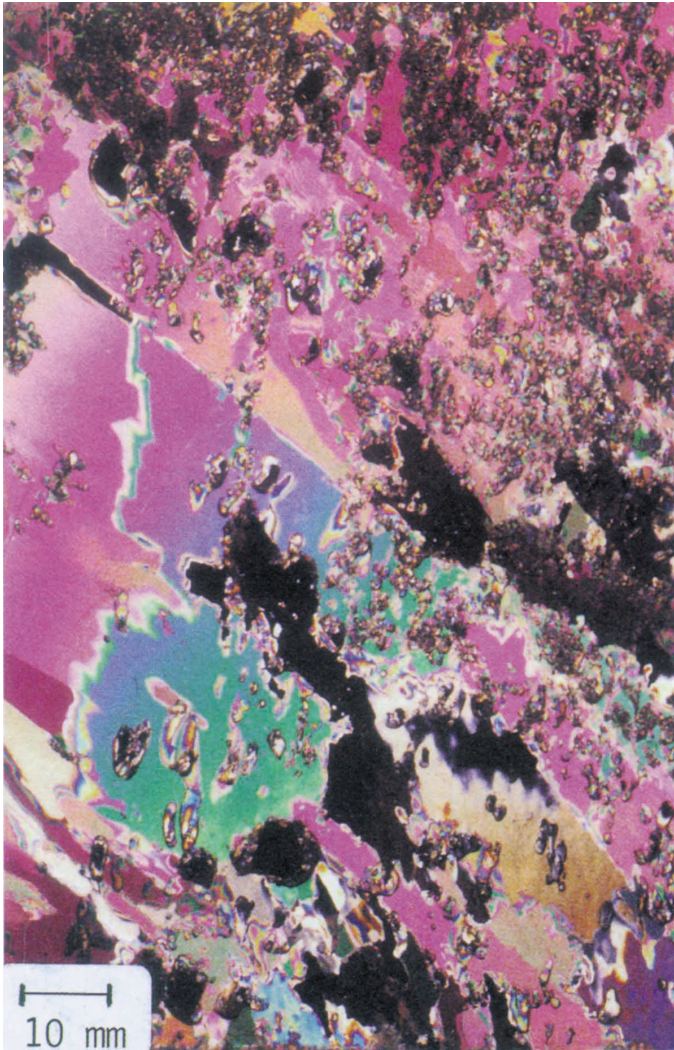
FIG. 6. Hummock core #3. Vertical section of the upper 140 mm depth, photographed between crossed polarizers.
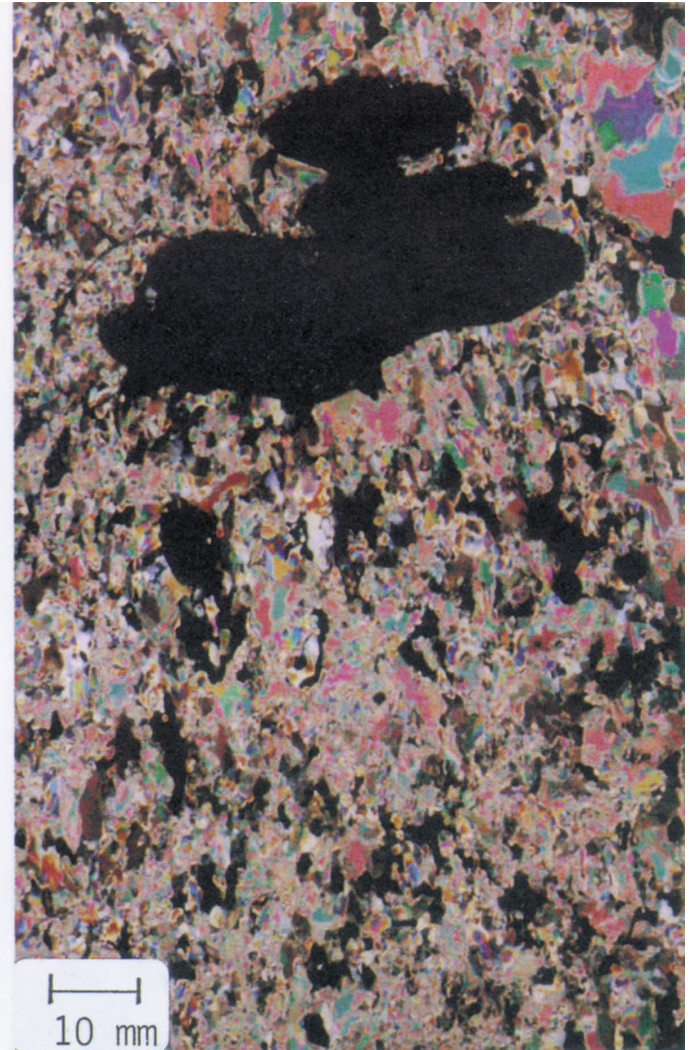
FIG. 7. Hummock core #4. Vertical section from 150 to 280 mm deep photographed between crossed polarizers.

shown in Fig. 8c. The vertical section exhibits three layers of distinct structure. The top layer, about 40 mm in thickness, is comprised of numerous small grains about 1 mm in diameter. This vertical section, in conjunction with the horizontal section at 20 mm (not shown), indicated that the ice was isotropic and equiaxial. This type of ice develops from freezing of saturated snow, and is called "snow ice" or granular ice. Air entrapped between snow particles evolves into nearly spherical inclusions, depicted as large bright objects in Fig. 8b. Their average diameter is 4 mm. These inclusions are consistently observed in, and confined only to, snow-ice layers in melt pond ice. Compared to commonly observed bubbles in hummock ice, they are more isotropic in shape, well separated, and have larger diameters.
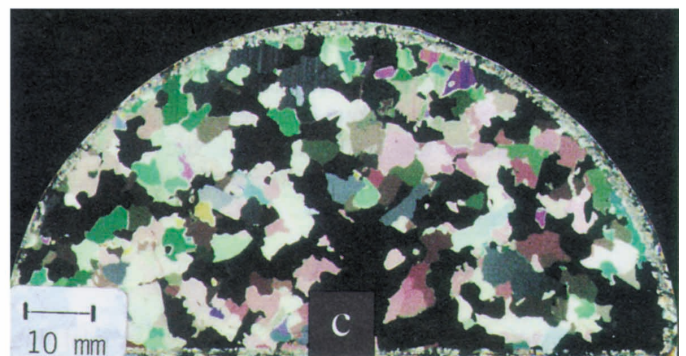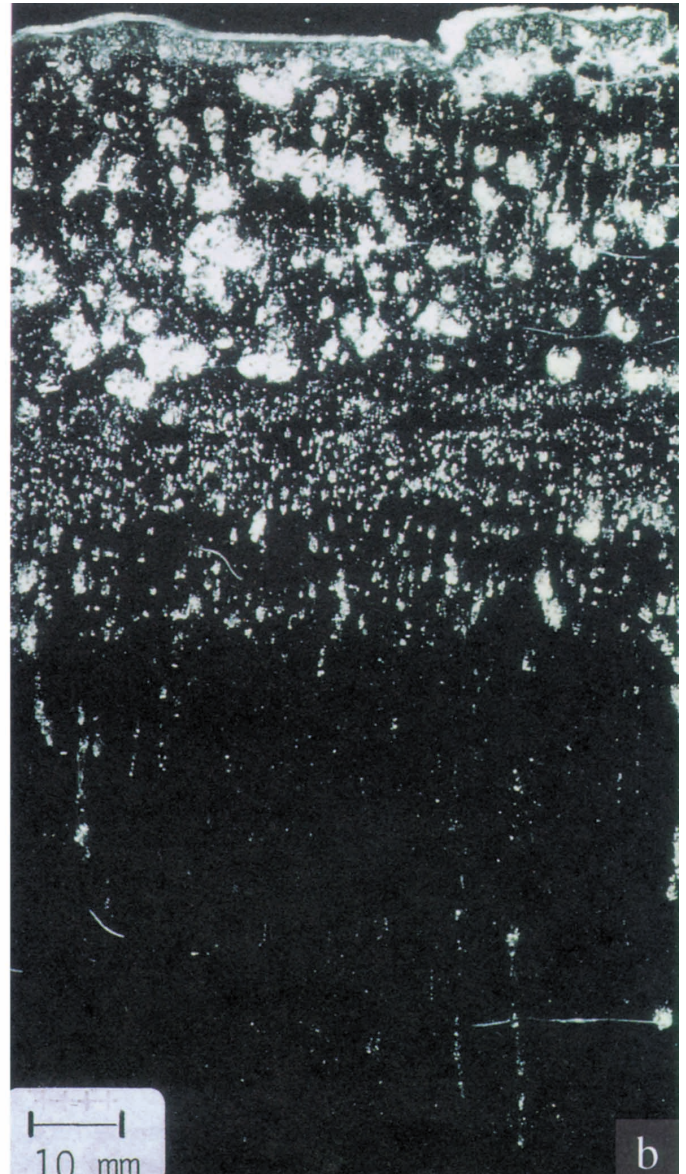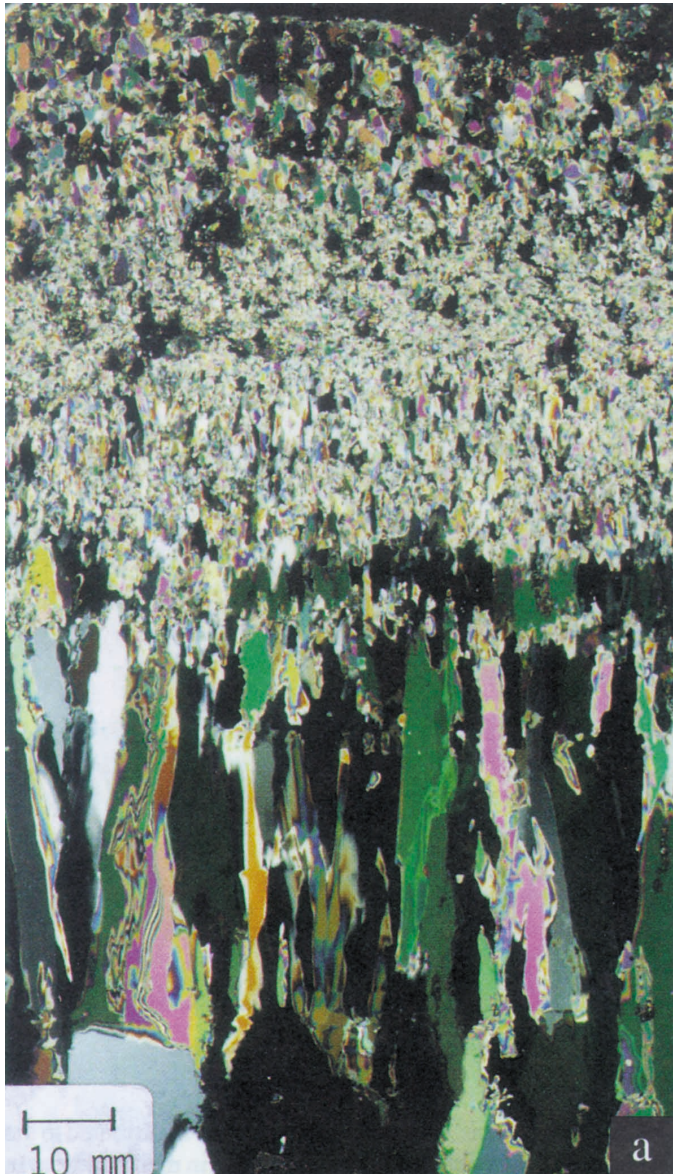
The middle layer, 25 mm thick, comprises ice crystals formed during the selection process, where crystals will survive only if their basal plane is parallel to the growth direction or the direction of maximum heat flow. Smaller air bubbles, ranging from a fraction of a millimetre to slightly above 1 mm, are readily visible in this layer (Fig. 8b). They are probably formed from air rejected by water during the formation of fine-grained crystals (i.e., not

instigated by percolation during summer melt). This type of bubble was found consistently in melt pond ice, mostly around small ice crystals. The coexistence of the two types of air inclusions should be considered in microwave scattering models. The top and the middle layers contain newer ice, formed subsequent to a melt season.

The third layer, about 100 mm below the surface, exhibits clear, nearly inclusion-free columnar-grained ice. The grains may appear to be of fresh water origin but the non-planer or the slight irregularity of their boundaries (Fig. 8c) suggests that the ice grew from brackish water. Measured salinity at depths where this layer exists ranges between 1.1 and 1.4 ppt.

Fig. 9 shows a vertical section from 150 to 270 mm depth from core #2. The core consisted of a 230 mm layer of non-saline snow-ice with grain diameters less than 2 mm. This suggested that ice was formed from water-saturated snow cover when numerous nucleators (snow particles) had existed. Air inclusions of the type observed in snow ice are clearly visible in Fig. 9b. Their diameters range from 1.5 to 6 mm. Small air bubbles, typically less than 1 mm diameter, can also be seen. The snow-

FIG. 8. Melt pond core #1. (a), (b) vertical section of the upper 140 mm depth photographed between crossed polarizers and in diffuse light respectively, (c) horizontal section at 90 mm depth photographed between crossed polarizers.

ice layer is underlain by a 30 mm transition layer of larger grains whose length varies between 1 to 4 mm. The layer marks a transition between the fine snow crystals and the columnar grains that represent originally saline ice which has been re-textured by aging (see the bottom of Fig. 9a). The establishment of columnar-grained ice also establishes the growth condition under which the impurities can be pushed down to the ice/water interface. Note the smooth transition in the grain structure in Fig. 9a. As for air inclusions, note the sharp boundary between the columnar-grained ice and the upper layers.

Careful examination of an individual air inclusion of the large diameter type (Fig. 9a), shows that its overall dark appearance is, in fact, cloudy with fading colours. The colours denote the presence of fine crystals within the inclusion. This supports the premise that the inclusions have originated from larger air pockets entrapped between snow particles during the freezing process.

A vertical section of the upper 140 mm depth from core #3 is shown in Fig. 10. The section consists of a saline snow-ice layer of average salinity 5.5 ppt and grain dimensions from 1 to 4 mm

(the grain structure is not shown in the figure). This layer extends to 170 mm and is underlain by columnar ice of less salinity, around 1 ppt. The relatively high salinity indicated that, prior to the latest freezing season, the pond was either connected to the
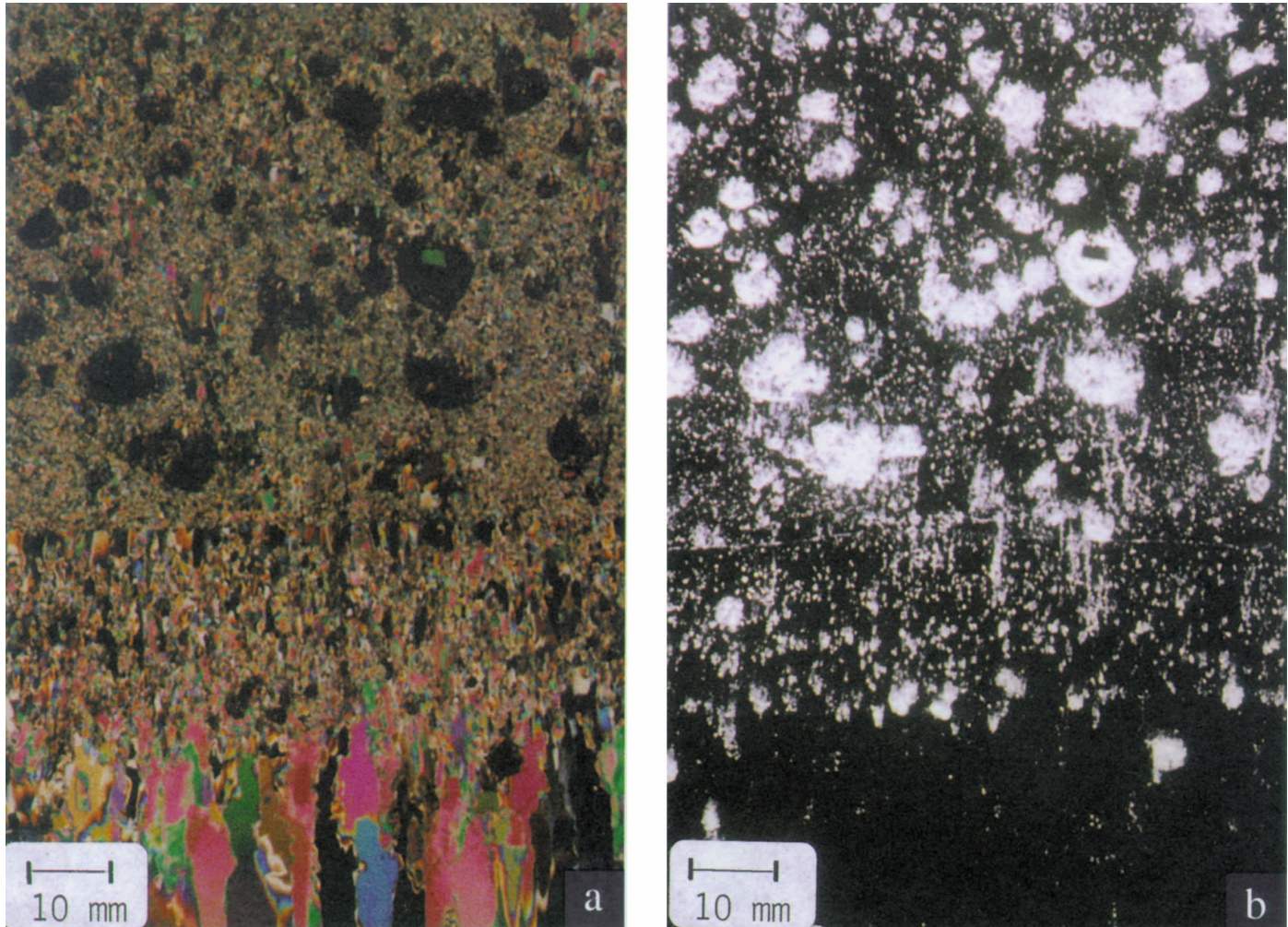
FIG. 9. Melt pond core #2. Vertical section of a depth range 150 mm to 270 mm photographed (a) between crossed polarizers, (b) in diffuse light.

seawater through a thaw hole, or filled with seawater as the surface was below the freeboard of the ice floe. The vertical needles shown in Fig. 10 are brine pockets. The spherical bright objects are air inclusions of the type observed in snow ice as described above. The diameter of air inclusions varies from 2 to 8 mm, with small inclusions existing near the surface. Observations from this core indicate that microwave dielectric and scattering models should account for the co-existence of both air and brine inclusions in melt pond ice.

Statistics of Air Bubbles in Multi-Year Ice

Bubbles were identified in digital images of vertical thin sections from 5 hummock and 5 melt pond cores. A total of 1496 bubbles from melt pond ice and 520 bubbles from hummock ice were identified. The smallest bubble that can be identified has a diameter of 0.1 mm. Bubble statistics were derived from three parameters: the circle equivalent diameter, the normalized compactness factor, and the distance to the nearest bubble. The statistics are included in Table 1. The average diameter of air bubbles in melt pond ice is 2.58 mm, which is slightly larger than that in hummock ice, 2.36 mm. The difference is attributed to the

presence of large bubbles of snow-ice origin in melt pond ice. In fact, the average diameter of that bubble type is 4.8 mm. The normalized compactness factor (C) is around 0.65 for both ice types, indicating that the overall bubble shape is similar in both types. Nevertheless, bubbles of snow-ice origin in melt pond ice

TABLE 1: Geometrical properties of air bubbles in multi-year ice

Ice type	Parameter	Mean	Median	Standard Deviation
melt pond	D (mm)	2.58	2.00	1.96
	C	0.62	0.65	0.19
	d (mm)	4.03	3.81	1.73
hummock	D (mm)	2.36	2.29	0.83
	C	0.68	0.69	0.12
	d (mm)	—	—	—

D, circle-equivalent diameter; C, compactness factor; d, distance between nearest bubbles.

are more spherical, with an average C = 0.83. The average distance to the nearest bubble in melt pond ice is 4.03 mm. This distance was not calculated for bubbles in hummock ice since most bubbles were detected manually due to their significant

overlap. Therefore, bubble sampling was not random and the calculated distance statistics should not be considered representative of the population.

Histograms of the three parameters are shown in Fig. 11. The circle-equivalent diameter histogram features a long tail for melt pond ice data; a manifestation of existence of the two bubble
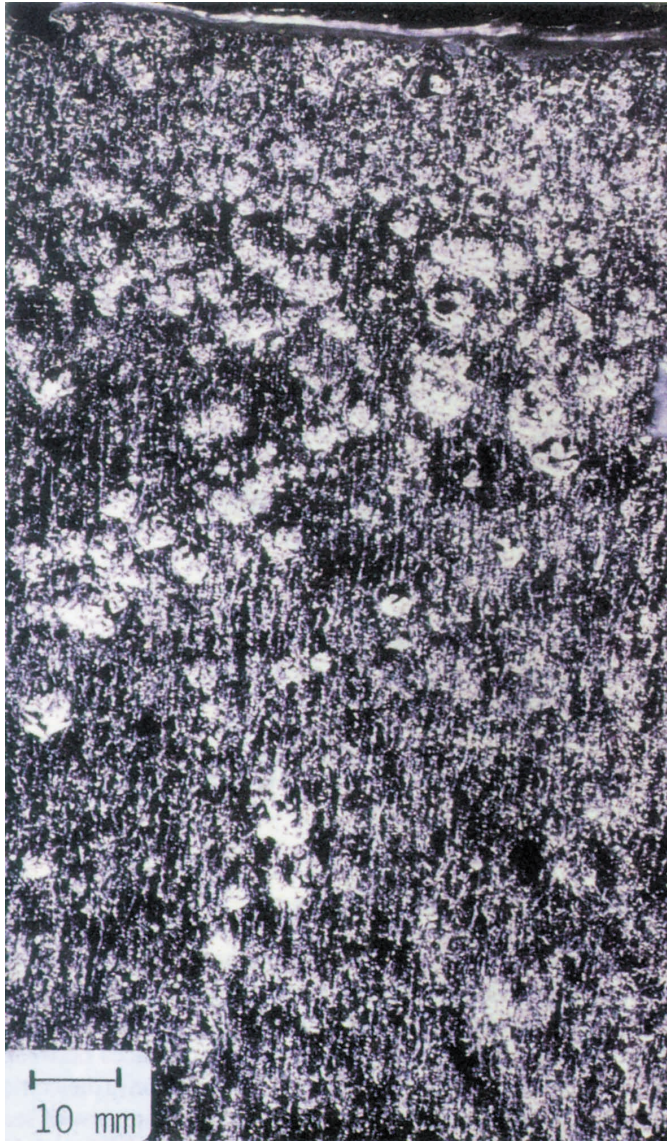

FIG. 10. Melt pond core #3. Vertical section of the upper 140 mm depth photographed in diffuse light.
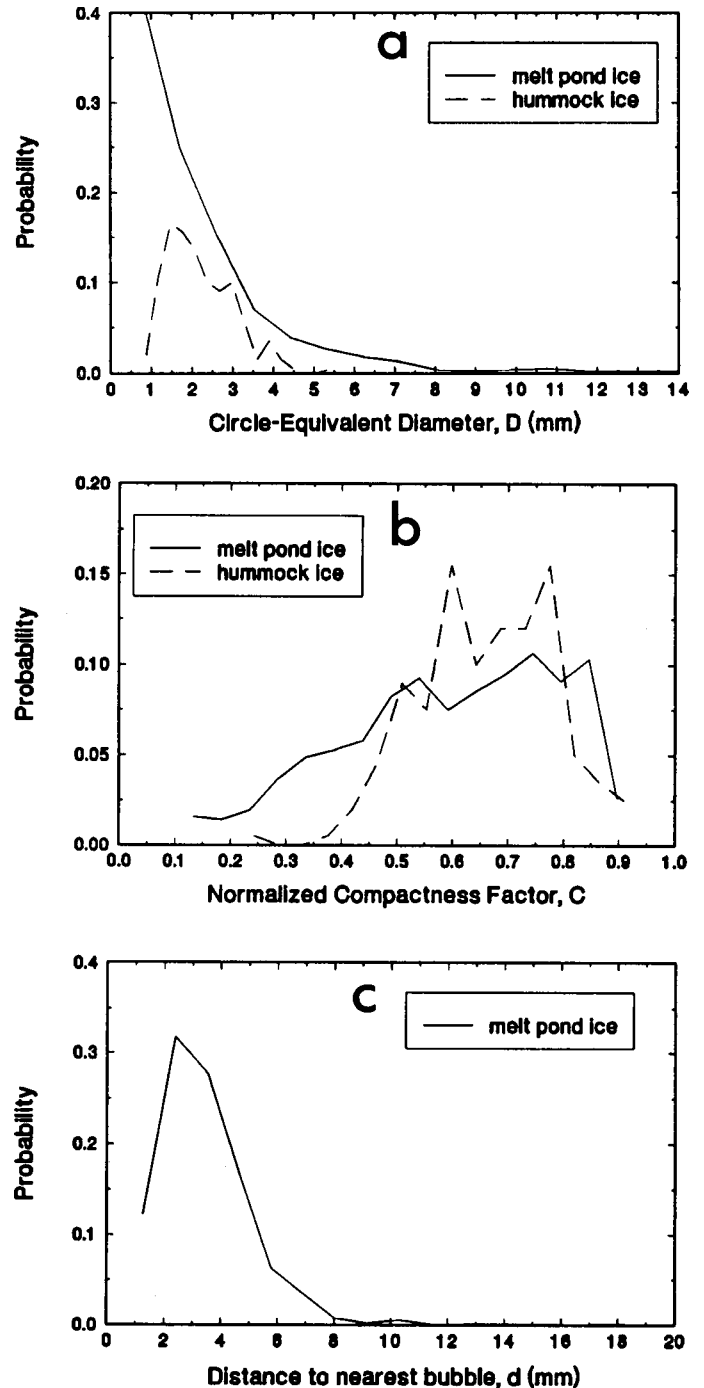

FIG. 11. Histograms of geometrical parameters of air bubbles in multi-year ice (a) circle-equivalent diameter, (b) normalized compactness factor, (c) distance to the nearest bubble.

types as suggested above. The compactness factor histograms show that melt pond ice contains inclusions of more elongated shapes (i.e., of small compactness factor). Moreover, bubbles in hummock ice have a rather limited variety of shapes as compared to bubbles in melt pond ice. The distance to the nearest bubble is characterized by a skewed histogram (from melt pond ice data only); this is evidence of the clustered bubble distribution pattern. The probabilities shown in Fig. 11 are important as a statistical description of bubbles in multi-year ice for the purpose of modeling microwave volume scattering models.

The probability of bubble existence at different depths is shown in Fig. 12 for melt pond ice data. Again, due to the interactive method of bubble detection in hummock ice (i.e., the biased sampling approach), the corresponding probability for hummock ice data was not obtained. A trend of bubble density decrease with depth is evident in the figure. The ragged appearance of the plot is probably caused by the limited number of samples. More samples are required to account for the large variability of the bubble-rich layer thickness.
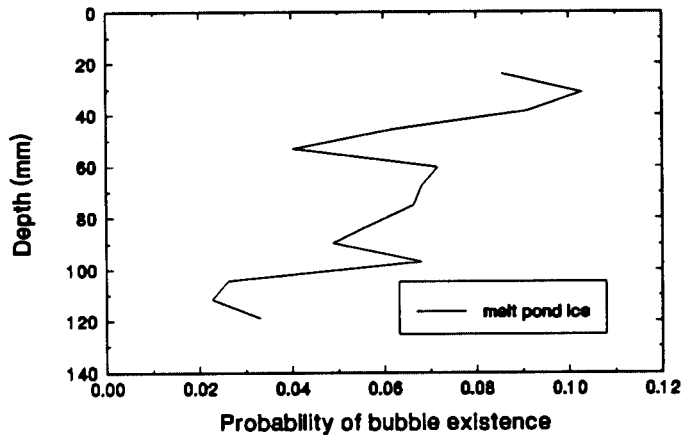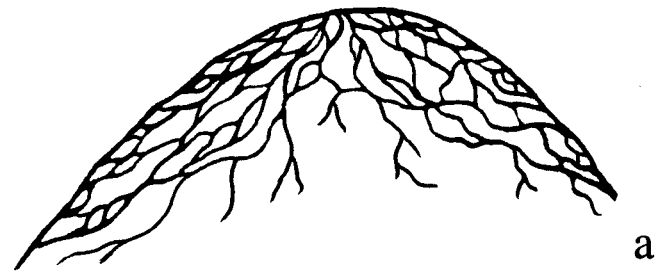
FIG. 12. Probability of occurrence of air bubbles in melt pond ice.

Air Bubble Formation in Multi-Year Ice

Based on observations from this study, a scenario of bubble formation in multi-year ice is introduced. The validity of the proposed ideas is limited to the present observations and should be established against other observations since variation of ice properties and natural ice formation conditions are diverse.

Considerable ablation of the surface of multi-year ice takes place in summer. Hummock surfaces are exposed to more solar radiation and will melt a significant amount of water. Also, melt water accumulating in melt ponds will decrease albedo, increase shortwave absorption, and will probably melt a significant amount of the ice beneath it. About 1 m of ice was observed to melt on a multi-year floe in Sabine Bay, Melville Island during the summer of 1992 (Rajan, pers. comm. 1993). Thus, there is much drainage through the remaining ice. In order for surface melt water to penetrate ice volume, a drainage network must be established. This is feasible only if channels can have their end points connected to the atmosphere. The convex surface of a hummock makes this possible (Fig. 13a). The surface melt penetrates ice and flushes salts. As the freezing season approaches, surface melt slows down while the water in channels continues to drain by gravity. Hence, channels will be partially empty. At freezing time, the empty parts become what are known as air inclusions. In other words, bubbles at or near the surface are formed from the remains of water drainage channels established in summer. This scenario explains the two commonly-observed geometrical features of air bubbles in hummock ice. The first is their orientation nearly parallel to the vertical plane or the gravity axis. The second is their interconnected nature near the surface.

The concave surface of melt pond ice does not allow formation of a drainage network in a significant manner. In this case, surface melt could accumulate, along with snow and rainwater, on top of the ice surface (Fig. 13b). At freezing time this layer consolidates forming a "newer" ice layer that could consist of a snow-ice layer if snow fall occurs immediately before freezing. Formation of air inclusions in snow-ice is possible through two means. The first is air entrapment between snow particles; the second is air trapped in the water or dissolved air rejected from water during ice freezing.

Hummock Ice:

- Drainage network can be established
- Bubbles are formed from remains of drainage network.

Melt Pond Ice:

- Drainage channels cannot be established
- Surface melt, snow and rain accumulate, and later consolidate to form a new ice layer.

FIG. 13. Multi-year ice surface conditions during summer melt (a) Hummock surface and (b) Melt pond surface. Conditions lead to different mechanisms of air bubble formation mechanisms.

Microwave Volume Scattering

An array of volume scattering models that apply to sea ice has been produced in the last two decades. Models are based on different realizations of ice and snow media, ranging from the number of scattering layers, the nature of interfaces between layers (rough or planar), and the type and distribution of dielectric inhomogeneities (scatterers) in ice. An extensive review of sea ice microwave volume scattering models is presented in Winebrenner *et al.,* (1992). A common approach adopted in these models is based on the concept of discrete scatterers (Kim *et al.,* 1984; Tsang and Ishimaru, 1987). In this approach, scattering is assumed to be caused by geometrically distinct scatterers of identical dielectric constant embedded in a host material of different dielectric constant. This two-phase approach is particularly useful in the case of multi-year hummock ice where clearly identifiable air bubbles are present in a background of desalinated ice of low electromagnetic absorption. Information on shapes, sizes, and spatial distribution of scatterers is necessary to initiate these models. Kim *et al.* (1984) used a semi-empirical model based on the assumption that scatterers are randomly distributed spheres of constant diameter. Winebrenner *et al.,*

(1989) evaluated a radiative transfer model based on the same assumption. Their analyses show a strong sensitivity of scattering cross section to air bubble radius. For example, backscatter coefficient increases by 4 dB as bubble radius increases from 0.5 to 1.0 mm. This implies that accurate information on bubble size is required.

Melt pond ice is characterized by a great variety of bubble size. The smallest bubble diameter that can be detected using the technique described above is 1 mm. However, based on the histogram of bubble diameters (Fig. 11a), it can be inferred that a large number of smaller bubbles exist in melt pond ice. Scattering from small bubbles, less than approximately 2 mm, can be modeled as Rayleigh scattering (Kim *et al.,* 1984; Drinkwater, 1989). The average circle-equivalent diameters in hummock and melt pond ice, 2.36 mm and 2.58 mm respectively, are almost equal to what is normally considered in microwave discrete scatterer models. The deviation from this value is larger for bubbles in melt pond ice (SD = 1.96 mm) as compared to bubbles in hummock ice (SD = 0.83 mm). The assumption of spherical air bubbles in multi-year ice, commonly employed in discrete scattering models, such as dense medium radiative transfer (Tsang and Ishimaru, 1987), is generally valid. Bubble shapes, however, deviate from a sphere, especially in the top (low density) layer of hummock ice. In that layer, bubbles are heavily connected and difficult to characterize. Ice can best be described as a continuous random medium in which permittivity is a random function of position. Stogryn (1987) has developed a model to calculate the effective permittivity and Winebrenner *et al.,* (1992) summarized available theories of microwave scattering in a random medium.

The coexistence of air inclusions and brine pockets in melt pond ice indicates that the assumption made in many dielectric and scattering models that multi-year ice is characteristically low-loss dielectric media with one inclusion/scattering element type (i.e., air bubbles) is not valid. Melt pond ice could have a wide variety of ice types and salt content. If a melt pond is connected to the sea water, under the floe, then highly saline, first-year type ice will exist on top of the pond in the winter. In this case models should account for the presence of three phases: pure ice, brine, and air bubbles.

Findings from this study signify five possible reasons for the variability of microwave volume scattering from multi-year ice. They contribute to differences in scattering levels that can explain the texture-rich signature of multi-year ice in SAR images (Holmes *et al.,* 1984; Barber and LeDrew, 1991; Shokr, 1991; Nystuen and Garcia, 1992; Rignot and Kwok, 1993). The first is the intrinsic difference between air bubble characteristics in hummocks and melt ponds. In hummock ice, air bubbles delineate a trail of drainage channels where water from surface melt percolates through ice. In melt pond ice, the surface layer is often composed of snow ice. This is where most of the air inclusions, believed to have originated from air entrapped between snow particles, exist. These inclusions are larger and more geometrically isotropic than bubbles in hummock ice. The second is the bubble orientation (both major axis of individual bubbles and their spatial arrangement) which follows mostly the predominant grain orientation. This is observed only when

multi-year ice has evolved from saline first-year ice. Variability of microwave scattering is inevitable since air bubble orientation varies relative to the fixed radar look and incidence angles (in case of SAR). The third is the possible existence of a saline melt pond surrounded by desalinated hummock ice. Saline melt ponds absorb more microwave energy and therefore return less volume scattering. Desalinated and bubbly hummocks allow more energy penetration and more volume scattering. The fourth is the formation of a newer snow-ice layer on top of the original ice in melt ponds. This layer, if present, is characterized by relatively large bubbles as described above. Although not statistically established, the present results indicate that the layer's thickness varies considerably, contributing to the variability of volume scattering. The fifth reason is the variability in depth of the bubble-rich layer in hummock ice. The present data show that this layer varies between a few millimetres to approximately 350 mm.

SUMMARY AND RECOMMENDATIONS

Basic information on crystalline structure, brine and air inclusions in Arctic sea ice was obtained from qualitative analysis of ice thin-section photographs. Statistics on size and shape of air bubbles in multi-year ice were also obtained from digital analysis of the photographs.

First-year ice features typically a thin layer (a few centimetres) of snow or frazil crystals, underlain by columnar crystals. Spherical brine pockets are observed within fine-grained ice structure. Needle-shaped brine pockets are observed within vertically-oriented frazil ice and columnar-grained ice. The pockets are parallel to the ice growth direction, which is mostly vertical. Spherical pockets are also found in sub-surface layers where columnar ice growth is interrupted by the presence of snow-like crushed ice and frazil ice.

Analysis of multi-year ice crystal structure confirmed the well-established conclusion that hummock and melt pond ice are structurally different. Hummock ice has a large columnar structure starting immediately under the surface. Melt pond ice is more likely to contain snow ice in the surface layer, formed from freezing of snow slush or waterlogged snow, on top of pre-existing ice. Air bubbles are different between hummock and melt pond ice in terms of their formation mechanism and geometrical characteristics. In hummock ice, bubbles are formed as a result of water percolation from surface melt during summer. They retain complicated, highly interconnected shapes near the surface and simpler, well separable shapes at larger depths. They measure typically 1-5 mm. In melt pond ice, two types of air inclusions whose characteristic dimensions differ by an order of magnitude exist. The first type is observed in snow-ice layers commonly existing near the surface. It probably originates from air entrapped between snow grains when snow slush, originally deposited on top of the pre-existing pond ice, is consolidated. These inclusions are nearly spherical with diameters between 3 to 10 mm, independent of depth. The second type is observed in fine-grained structure (snow-ice, frazil, or transition columnar ice). It features small bubbles with typical diameters around

1 mm. Their origin is believed to be air trapped or rejected during ice formation on top of pre-existing melt pond ice surface.

In the top (low density) layer of hummock ice, bubbles tend to lose their individual entity and form a complicated network. In this case, ice can best be described as a continuous random medium in which permittivity is a random function of position. In some melt pond cores, two inclusions, brine pockets and air bubbles, are observed. In this case, the conventional representation of multi-year ice as a two-phase medium of pure ice and air bubbles, may not be appropriate. A more realistic three-phase model should be considered.

A variety of grain structures and inclusion patterns are found in cores collected from same area (roughly 300×300 m) in the same multi-year ice floe. This raises a question on the spatial variation of ice structural properties in relation to the observed microwave scattering signal. The variation should be addressed on a statistical basis in a future study.

A realistic physical model of multi-year ice should take into account not only statistical characteristics of its microstructure including inclusions, but also probabilistic occurrence of hummocks and melt ponds within a given floe. This requires an appropriate survey to determine characteristics of floe surface topography, followed by a proper core sampling scheme which reflects those characteristics. A future experimental program should be designed to fulfill this requirement. The present results can be used to test and revise assumptions employed in dielectric and microwave scattering models.

ACKNOWLEDGEMENTS

REFERENCES

BARBER, D.G., 1991. The seasonal sea ice monitoring site (SIMS) 1991 science plan. Technical Report ISTS-EOL-SIMS-TR91-001. Earth Observation Laboratory, Institute for Space and Terrestrial Science, University of Waterloo, Waterloo, Ontario, Canada.

BARBER, D.G., and LeDREW, E.F. 1991. SAR ice discrimination: A multivariate approach. Photogrammetric Engineering and Remote Sensing 57(4):385–395.

BJERKELUND, C.A., LAPP, D.J., RAMSEIER, R.O., and SINHA, N.K. 1985. The texture and fabric of the second year sea ice cover at Mould Bay, Prince Patrick Island, NWT, April 1983. Proceedings of the International Geoscience & Remote Sensing Symposium (IGARSS'85), University of Massachusetts, Amherst, MA. 426–431.

COX, G.F.N., and WEEKS, W.F. 1975. Brine drainage and initial salt entrapment in sodium chloride ice. Hanover, New Hampshire: U.S. Cold Regions Research and Engineering Laboratory, Research Report 345.

DeLOOR, G.P. 1968. Dielectric properties of heterogeneous mixtures containing water. Journal of Microwave Power 3: 67–73.

DRINKWATER, M.R. 1989. LIMEX'87 ice surface characteristics: Implications for C-band SAR backscatter signatures. IEEE Transactions on Geoscience & Remote Sensing GE-27(5): 501–513.

EICKEN, H., and ANGE, M.A. 1989. Development and properties of sea ice in the coastal regime of the Southeastern Weddell Sea. Journal of Geophysical Research 94(C6):8193–8206.

EICKEN, H., LANGE, M.A., and ACKLEY, S.F. 1990. Quantification of sea-ice textures through automated digital image analysis. Hanover, New Hampshire: Cold Regions Research and Engineering Laboratory, Monograph 90–1. 28–32.

FUNG, A., and EOM, H. J. 1982. Application of a combined rough surface and volume scattering theory to sea ice and snow backscatter. IEEE Transactions on Geoscience and Remote Sensing GE-20(4):528–536.

GOGINENI, S., MOORE, R.K., WANG, Q., GOW, A., and ONSTOTT, R.A. 1990. Radar backscatter measurements over saline ice. International Journal of Remote Sensing 11(4): 603–615.

HOLMES, Q.A., NUESCH, D. R., and SCHUCHMAN, R. A. 1984. Textural analysis and real-time classification of sea ice types using digital SAR data. IEEE Transactions on Geoscience and Remote Sensing GE-22(2):113–120.

KIM, Y.S., MOORE, R.K., and ONSTOTT, R.G. 1984. Theoretical and experimental study of radar backscatter from sea ice. Lawrence, Kansas: Remote Sensing Laboratory, University of Kansas. Technical Report. 331–37.

LIVINGSTONE, C.E., SINGH, K.P., and GRAY, A.L. 1987. Seasonal and regional variation of active/passive microwave signatures of sea ice. IEEE Transactions on Geoscience and Remote Sensing GE-25(2):159–173.

NAKAWO, M., and SINHA, N.K. 1981. Growth rate and salinity profiles of first-year sea ice in the High Arctic. Journal of Glaciology 27(96):315–330.

———. 1984. A note on brine layer spacing of first-year sea ice. Atmosphere/Ocean 22(2):193–206.

NICHOLS, A.D., WILHELM, J.W., GAFFIELD, T.W., INKDTER, R.D., and LEUNG, S.K. 1986. A SAR for real-time ice reconnaissance. IEEE Transactions on Geoscience and Remote Sensing GE-24(3):383–389.

NYSTUEN, J.A., and GARCIA JR., W. 1992. Sea ice classification using SAR backscatter statistics. IEEE Transactions on Geoscience and Remote Sensing 30(3):502–509.

ONSTOTT, R.G. 1992. SAR and scatterometer signatures of sea ice. In: Carsey, F.D., ed. Microwave remote sensing of sea ice. Geophysical Monograph 68, American Geophysical Union. 73–104.

PEROVICH, D.K., and GOW, A.J. 1991. A statistical description of the microstructure of young sea ice. Journal of Geophysical Research. 96(C9):16943–16953.

PEYTON, H.R. 1966. Sea ice strength. Fairbanks, Alaska: Geophysical Institute, University of Alaska. Technical Report, UAGR-182.

POE, G.A., STOGRYN, A., EDGERTON, A.T., and RAMSEIER, R.O. 1974. Study of microwave emissive properties of sea ice. Azusa, California: Aerojet Electrosystems Co. Technical Report, 1804FR-1.

REDDAN, S.P., BARBER, D.G., and LeDREW, E.F. 1991. SIMMS'91 data report. Technical Report ISTS-EOL- SIMS-TR91-005. Earth Observation Laboratory, ISTS, University of Waterloo, Waterloo, Ontario, Canada.

RIGNOT, E., and KWOK, R. 1993. Characterization of spatial statistics of distributed targets in SAR data. International Journal of Remote Sensing 14(2):345–363.

SHOKR, M.E. 1991. Evaluation of second-order textural parameters for sea ice classification from radar images. Journal of Geophysical Research 96(C6):10625–10640.

SHOKR, M.E., and SINHA, N.K. In press. Physical, dielectrical and microstructural properties of Arctic sea ice observed during SIMMS'92 field experiment. Research Report #MRB, Atmospheric Environment Service, Toronto, Canada.

SINHA, N.K. 1977. Technique for studying structure of sea ice. Journal of Glaciology 21:385.

———. 1984. Uniaxial compressive strength of first-year and multi-year sea ice. Canadian Journal of Civil Engineering 11: 82–91.

———. 1986. Young Arctic frazil ice: field and laboratory strength tests. Journal of Materials Science 21(5):1533–1546.

STOGRYN, A. 1987. An analysis of the tensor dielectric constant of sea ice at microwave frequencies. IEEE Transactions on Geoscience and Remote Sensing GE-25(2):147–158.

TSANG, L., and ISHIMARU, A. 1987. Radiative wave equations for vector electromagnetic propagation in dense nontenuous media. Journal of Electromagnetic Wave Applications 1(2): 161–175.

TUCKER III, W.B., GOW, A.J., and WEEKS, W.F. 1987. Physical properties of summer sea ice in the Fram Strait. Journal of Geophysical Research 92(C7):6787-6803.

TUCKER III, W.B., GRENFELL, T.C., ONSTOTT, R.G., PEROVICH, D.K., GOW, A.J., SHUCHMAN, R.A., and SUTHERLAND, L.L. 1991. Microwave and physical properties of sea ice in the winter Marginal Ice Zone. Journal of Geophysical Research 96(C3): 4573–4587.

ULABY, F., MOORE, R.K., and FUNG, A.K. 1986. Microwave Remote Sensing. Vol II. Washington, D.C.:Artech House, Inc.

VANT, M.R., RAMSEIER, R.O., and MAKIOS, V. 1978. The complex dielectric constant of sea ice at frequencies in the range of 0.1-40 GHz. Journal of Applied Physics 49(3):1264–1280.

WEEKS, W.F., and ACKLEY, S.F. 1982. The growth, structure, and properties of sea ice. Hanover, New Hampshire: Cold Regions Research and Engineering Laboratory, Monograph 82–1.

WEEKS, W.F., and ASSUR, A. 1963. Structural control of the vertical variation of the strength of sea and salt ice. In: Kingery, W.D., ed. Ice and snow; properties, processes, and applications. Cambridge, Massachusetts: M.I.T. Press. 258–276.

WEEKS, W.F., and GOW, A. J. 1978. Preferred crystal orientation in the fast ice along the margins of the Arctic Ocean. Journal of Geophysical Research 83:5105-5121.

WEEKS, W.F., GOW, A.J., KOSLOFF, P., and DIGBY-ARGUS, S. 1990. The internal structure, composition and properties of brackish ice from the Bay of Bothnia. Hanover, New Hampshire: Cold Regions Research and Engineering Laboratory, Monograph 90-1:5–15.

WEEKS, W.F., and LOFGREN, R. 1967. The effective solute distribution coefficient during the freezing of NaCl solutions. In: Oura, H., ed. Physics of snow and ice, Vol. 1, Part 1. Institute of Low Temperature Science, Hokkaido University, Japan. 579–597.

WINEBRENNER, D.P., TSANG, L., WEN, B., and WEST, R. 1989. Sea ice characterization measurements needed for testing of microwave remote sensing models. IEEE Journal of Oceanic Engineering 14(2):49–158.

WINEBRENNER, D.P., BREDOW, J., FUNG, A.K., DRINKWATER, M.R., NGHIEM, S., GOW, A.J., PEROVICH, D.K., GRENFELL, T.C., HAN, H.C., KONG, J.A., LEE, J.K., MUDALIAR, S., ONSTOTT, R., TSANG, L., and WEST, R.D. 1992. Microwave sea ice signature modeling. In: Carsey, F.D., ed.. Microwave remote sensing of sea ice. Geophysical Monograph 68, American Geophysical Union. 137–175.